Influence of topology and diode characteristics of AC-DC converters for low power piezoelectric energy harvesting

Kevin Nadaud, Guylaine Poulin-Vittrant, Daniel Alquier

Influence of topology and diode characteristics of AC-DC converters for low power piezoelectric energy harvesting

Kevin Nadaud*, Guylaine Poulin-Vittrant†, and Daniel Alquier‡

GREMAN UMR 7347, Université de Tours, CNRS, INSA-CVL, 16 rue Pierre et Marie Curie, 37071 Tours, France

June 1, 2021

Abstract

Most often, piezoelectric generators are connected to a AC-DC converter, also called rectifier, to obtain a continuous energy which can be regulated and stored. In the case of low power generators, the choice of the rectifier is critical since the losses into this circuit are not negligible and should be as low as possible.

In this paper, different topologies of rectifier using different diode references are studied to rectify the output voltage of a piezoelectric generator. We show that the differences between the fullwave rectifier and a voltage doubler are quite small in terms of output power. The main differences are visible on the final voltage value and the optimal load. On the contrary, the choice of diodes is critical, especially the reverse leakage current which must be limited since it largely affects the output power for low power generators.

The internal capacitance of the generator also plays an important role since it changes the capability of the generator to provide current. We show that low threshold voltage diodes are more appropriate for generators presenting a high internal capacitance while low leakage current are preferable for generators presenting a low internal capacitance value.

Keywords: energy harvesting, piezoelectric, modeling, rectifier

1 Introduction

To supply the ever-increasing number of portable devices, a tendency is to build generators, in particular piezoelectric ones (PG) to harvest the wasted mechanical energy which can have various origins (ambient vibrations, human body movements, etc.). In order to directly implement the lead-free directives, developments of nanomaterials such as ZnO nanowires have been investigated in PGs due to their piezoelectric properties and bio-compatibility [1–5]. PGs can be used to provide the electrical energy to devices such as sensors, actuators and wireless transmitters [6–9]. A temporary energy storage element may be needed, like a capacitor [10,11] or a small embedded battery [12,13]. In both cases, the PG must be connected to the storage element through

*Email: kevin.nadaud@univ-tours.fr ORCID: 0000-0002-2969-1453
†Email: guylaine.poulin-vittrant@univ-tours.fr ORCID: 0000-0003-0501-8122
‡Email: daniel.alquier@univ-tours.fr ORCID: 0000-0003-1345-8195

an AC-DC converter, also called rectifier, since the electrical output of the PG is alternative. The architecture of the rectifier is closely related to both the PG and the storage element. Various topologies have been proposed, from simple 4-diodes bridges [14], voltage multipliers [10] or more complex circuits using synchronized switch technique [15,16].

Even if some bridge-less topologies have been reported [17,18], they require an external controller for the switches whose consumption is not always taken into account for the efficiency calculation. A truly autonomous device must include a passive rectifier to provide the energy consumed by the control circuit of the active AC-DC converter.

In this paper, we focus mainly on passive rectifiers since they do not require energy to control electronic switches. Even if they present intrinsic losses due to diodes or passive components, passive rectifiers are appropriate when the total power supplied by the harvester is small, for example piezoelectric nanowires based device [1–5,19]

The goal of this paper is to study different topologies of AC-DC converter in order to find out the most suitable for low power energy harvesting. Moreover, the effect of the diode characteristics, forward voltage V_f and reverse current I_r, is also studied. For this purpose, different references of diode have been selected with various values of forward voltage and reverse current. The goal is here to know for a given energy source, which parameter is critical and which rectifier topology is suitable.

2 Materials and methods

2.1 Rectifiers and diodes

In this section, the two studied rectifier topologies and the characteristics of the chosen diodes are presented. The first rectifier is the well known fullwave rectifier based on 4 diodes as shown Fig. 1a. For this circuit, both polarities are rectified which increases the total amount of energy transmitted to the load compared to a single diode rectifier. The main drawback of this circuit is the diode voltage drop, since the threshold of the diodes is present twice. The consequence is a lower magnitude of the expected final voltage when the capacitor is fully charged compared to the initial alternative voltage, and also to the voltage, that would be obtained thanks to a single diode rectifier.

The second rectifier is the Latour voltage doubler as presented Fig. 1b. The advantage of this circuit is a lower voltage drop across the diode, which is present only one time for each polarity. In open circuit condition (resistive load R_L infinite), the voltage at the output of the circuit is close to twice the voltage magnitude at the input of the rectifier, and it is only diminished by the forward voltage drop of the diode. Similarly to the fullwave bridge, both polarities of the signal are rectified contrary to the simple rectifier. C_0 capacitors are just here to provide a mid-point

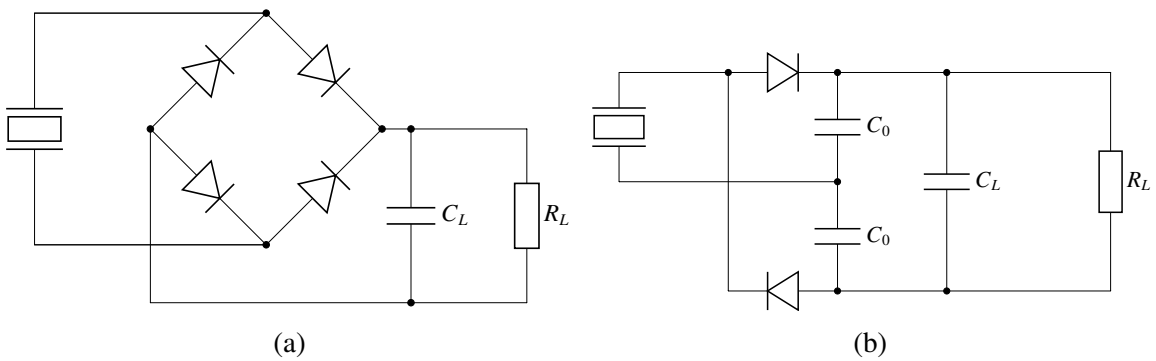

Figure 1: Studied rectifier, full wave bridge rectifier (a) and Latour voltage doubler circuit (b).

Table 1: Summary of the available diodes, ordered by increasing threshold voltage. Given values are typical from the datasheet at 25 °C.

		Reference			
	Condition	1PS76SB10	1PS79SB30	RB751S40	1N4148
V_f	I_f =100 uA	150 mV	190 mV	260 mV	500 mV
	I_f =10 mA	300 mV	310 mV	390 mV	750 mV
I_r	V_r =5 V	500 nA	130 nA	13 nA	5 nA
	V_r =20 V	1000 nA	280 nA	40 nA	12 nA

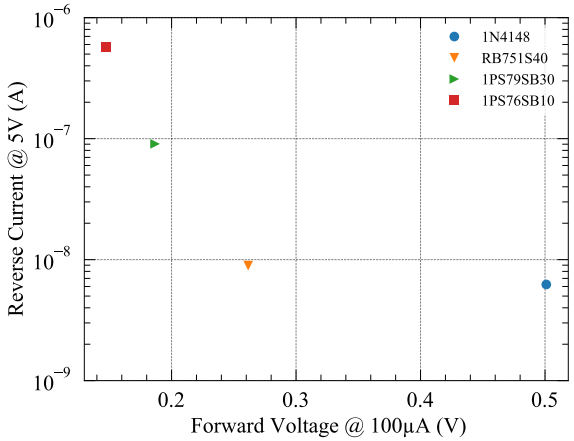

Figure 2: Reverse leakage current at 5 V as a function of the forward threshold voltage at 100 µA for the studied diodes.

to connect the second terminal of the generator, their values are small compared to the storage capacitor C_L.

The value of the storage capacitor has been chosen to have a usable voltage at the output of the AD-DC converter, i.e. a small voltage ripple in order to avoid the use of a voltage regulator. We choose a ceramic capacitor with a value of 1 µF, while and a larger value may be used if a lower ripple or higher stored energy are needed.

The aim of this part is to present the diode types that were chosen in this study. When choosing a diode there is a trade-off between (i) a low forward voltage when the diode is on, also called the threshold voltage, and (ii) a low reverse current when the diode is off, also called leakage current. These two parameters are linked together and decreasing the threshold voltage has the consequence to increase the leakage current. The selected diodes are three Schottky barrier diodes (1PS76SB10,1PS79SB30 and RB751S40) and one $p-n$ junction diode (1N4148). Table 1 summarizes the forward voltage and leakage current for the different diodes and Fig. 2 shows the reverse leakage current at −5 V as a function of the forward threshold voltage at 100 µA for the studied diodes.

Since the selected references are commonly used, the SPICE model of the diodes, given in supplementary material, can be easily found and have been downloaded from[20]. Fig. 3 shows the simulation results and the forward and reverse current as a function of the forward and reverse voltage for the different diodes at room temperature. For all diode references, there is a good agreement between datasheet results and simulations indicating that the electrical model describes correctly the diode behavior in forward and reverse conditions.

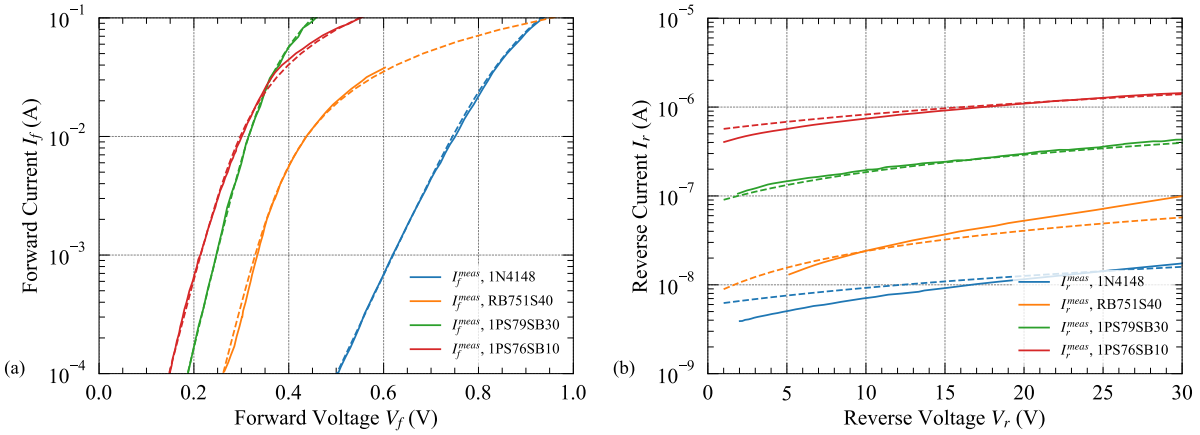

Figure 3: Forward (a) and reverse (b) currents as a function of the forward and reverse voltage respectively for different diodes at 25 °C. Full lines correspond to the datasheet values and dashed lines to the SPICE Model.

2.2 Simulation and experimental procedures

The study of the rectifiers has been made by both simulation and measurement. The electrical circuit simulations presented in this paper have been made using Xyce Electronic Simulator™[21], in the time domain. The PG has been modeled by a Thevenin equivalent generator, i.e. voltage source connected in series with an internal impedance.

The experimental test bench used to characterize the rectifier is shown Fig. 4. It consists of a 6517B Keithley electrometer, used in voltage mode, a variable resistive load and a capacitor. The excitation of the PG is applied using a mechanical shaker (LDS V406) driven by a power amplifier (LDS PA100E). A function generator (Tektronix AFG1022) is used to control the magnitude and frequency of the shaker. The considered piezoelectric generator is a PZT buzzer and its internal impedance has been measured using a custom impedancemeter as presented in ref.[22]. The force applied onto the PG has a magnitude of 3 N and a frequency of 5 Hz. A prestress has been adjusted to keep the contact during the full period of the mechanical excitation. An oscilloscope (MDO3014 Tektronix) is used to monitor the voltage at the output of the PG, the function generator output and the force magnitude. The applied force is monitored using a force sensor and the magnitudes of both the force and prestress are recorded in order to ensure that all the tests are performed in the same conditions. Electrical isolation between the sample and the mechanical structure of the test bench is made using glass slides.

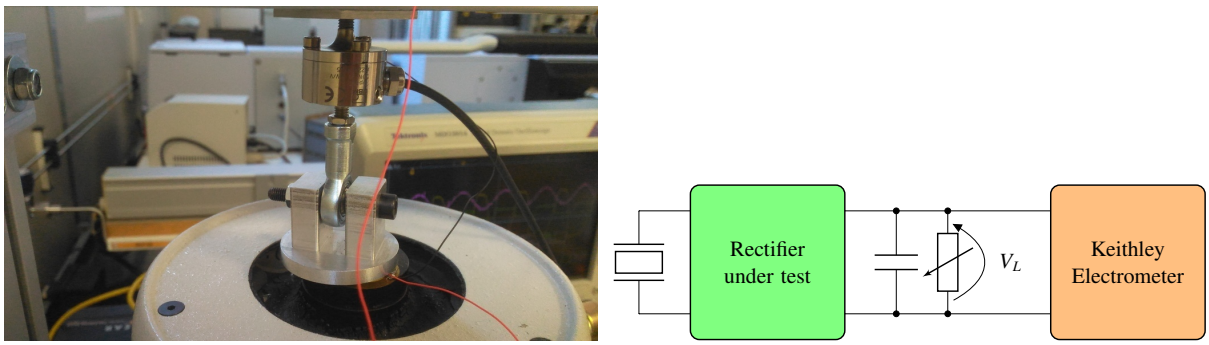

Figure 4: Description of the used test bench to characterize a rectifier.

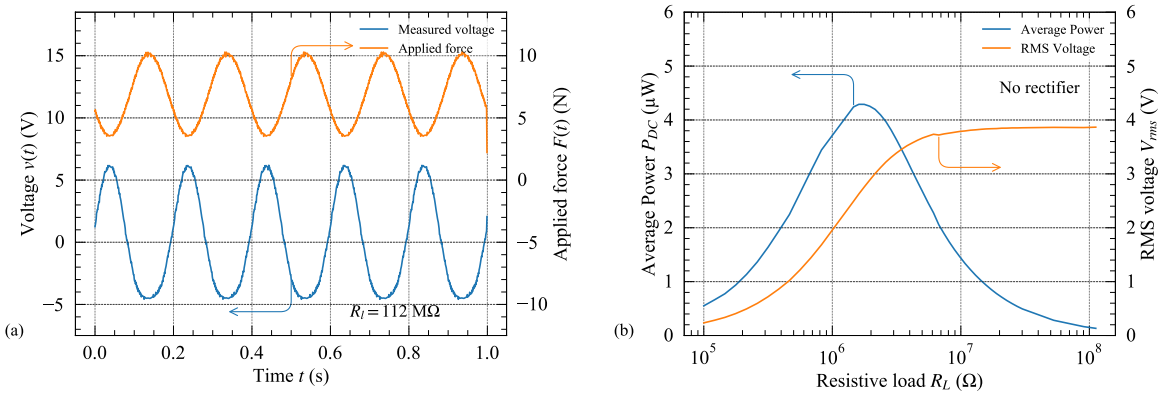

Figure 5: Applied force onto the PG as a function of time and voltage measured with a resistive load of 113 MΩ (a). RMS voltage and average power as a function of the resistive load for the same PG connected directly to a resistive load (b).

3 Results and discussion

In this experimental part, the PG is firstly characterized only with a resistive load in order to measure the voltage signal response and to identify the optimal load. In a second step, the PG is connected to a resistive load through different rectifier topologies and using different diode references. In this part, average voltage, DC power dissipated in the load and rising time starting from the discharged state to reach the steady state are studied in order to know the most suitable topology/diode couple.

3.1 Without rectifier

First, the PG has been characterized without rectifier. A simple resistive load, noted R_L, has been connected in order to identify the optimal load and the harvested power at this load. Fig. 5a shows the temporal waveforms of the applied force onto the PG and corresponding measured voltage across a resistive load of 113 MΩ. Even if the force is sinusoidal, the measured voltage is not perfectly sinusoidal which is attributed to the non-linear behavior of the PZT based PG, as the PG is under high level of strain. Using this temporal waveform, the RMS voltage can be computed for the given load and by changing the load, it is possible to obtain the RMS voltage and average power as a function of the resistive load.

Fig. 5b shows the RMS voltage and the average power as a function of the resistive load. The RMS voltage increases when the resistive load increases which is the expected behavior. The average power versus resistive load presents a maximum for a given resistance, called optimal load R_L^{ave} [22] This corresponds to the best compromise between two situations: (i) a high voltage for high value of resistance load but a small value of the current and (ii) a high current for small load value but a small voltage. In harmonic regime, the optimal load correspond to the modulus of the internal impedance and, in the case of a capacitive internal impedance, its value is known as :

$$R_L^{ave} = \frac{1}{C_{int}\omega_0} \tag{1}$$

where C_{int} is the internal capacitance of the PG and ω_0 is the angular frequency of the solicitation. With an internal impedance of 17.5 nF, the expected value of optimal load in our case is 1.82 MΩ, which very close to the measured value, 1.72 MΩ. The slight shift may be attributed to the presence of harmonics included in the open circuit voltage[22]. The power at optimal load

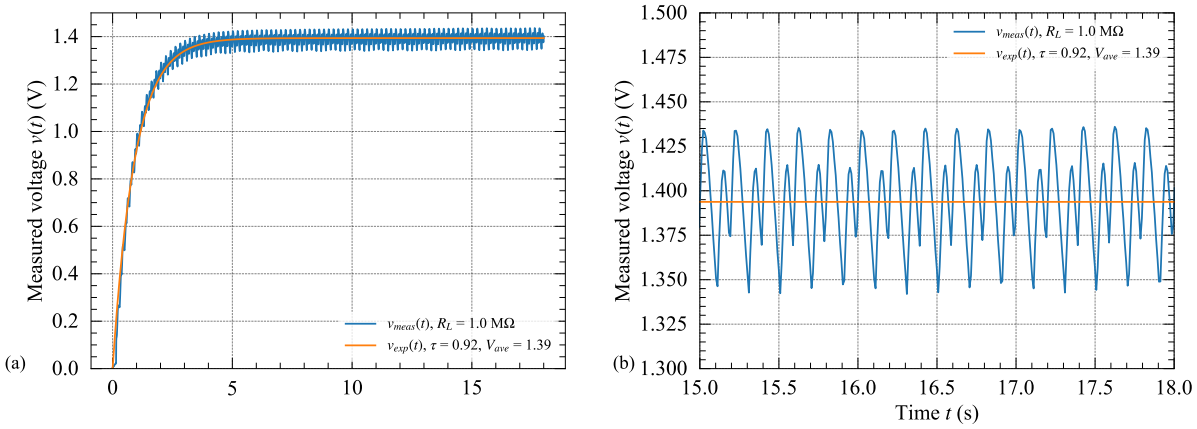

Figure 6: Typical charging curve of a capacitor of 1 µF using the fullwave rectifier using `RB751S40` diodes.

can be computed using the following expression:

$$P_{AC}^{max} = \frac{V_{OC}^2 C_{int} \omega_0}{4} \tag{2}$$

The measured value (4.29 µW) is closed to the theoretical value (4.08 µW).

3.2 Influence of rectifier topology and diodes

In this second section, the influence of both the rectifier topology and diode choice on the average power versus resistive load is presented. First, the average final voltage versus resistive load is presented since it corresponds to the steady state operation of the rectifier. Then, the effect of the topology and diode reference on the average power transmitted to the load is discussed. Finally, the effect of both the load and the rectifier topology, on the rising time starting from the discharged state to reach the steady state, is shown.

A typical measured charging curve is shown Fig. 6 which consists of the voltage across the capacitor and load as a function of the time. The voltage ripple corresponds to each half-wave which charges the storage capacitor. The low frequency component, similar to an exponential waveform, corresponds to the accumulation of energy into the capacitor. To measure the final voltage, only the steady state part is used from 10 s to 17 s in Fig. 6a. The average final voltage has been calculated using the following formula:

$$V_{ave} = \frac{1}{t_2 - t_1} \int_{t_1}^{t_2} v(t)\,\mathrm{d}t \tag{3}$$

In order to estimate the charging time of the capacitor, the curve has been fitted using the following function:

$$v_{exp}(t) = V_{ave}\left(1 - \exp\left(\frac{-t}{\tau}\right)\right) \tag{4}$$

τ corresponds to the rising time and V_{ave} to the mean value of the voltage when time tends to the infinity. The τ value is a simple indicator of the charging time necessary to reach a given percentage of the final value (i.e. 3τ for 95 %, 5τ for 99 %...). Thus the fitting of the curve provides metric in order to compare results obtained with different experimental conditions and different rectifiers. In this study, we only consider a purely resistive load in addition to the

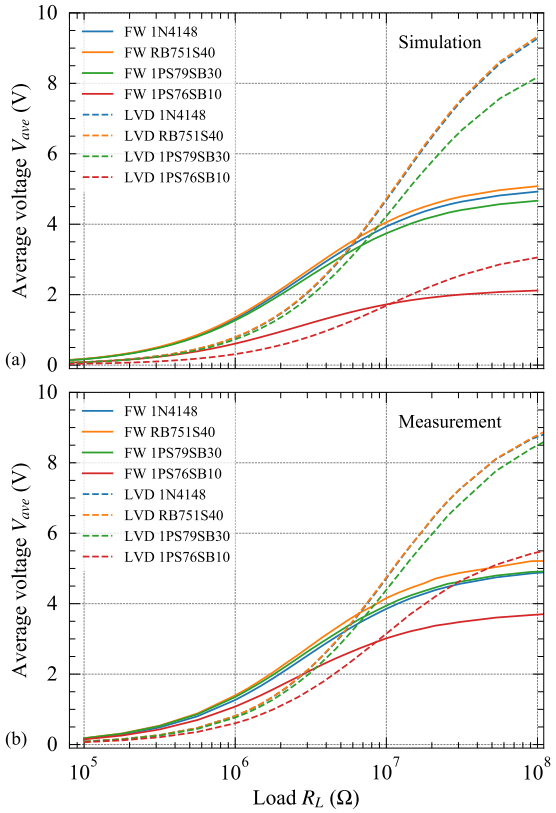

Figure 7: Final voltage as function of the resistive load for different rectifier topology and for two diode reference (a) in simulation (b) in measurement. `FW` stands for fullwave rectifier and `LVD` stands for Latour voltage doubler.

filtering capacitor. In the case of a real circuit, a DC-DC converter can be used in order regulate the voltage[14].

Fig. 7 presents the simulated and measured average voltage as a function of the resistive load value for different topologies of rectifier and references of diode. For all references of diode, the voltage at high load values is higher for voltage doubler than for the fullwave bridge, a factor 2 is visible which corresponds to the expectation. This means that the fullwave rectifier is more adapted to "low" load values than the voltage doubler.

Concerning the effect of the diode reference, similar results are visible on both topologies: the diode with the higher leakage current (and having the lower threshold voltage) provides a lower voltage. This is counter-intuitive because, in the case of the piecewise linear model, using a diode with a lower threshold voltage, the final voltage should be higher. Nevertheless, the reverse leakage current discharges the capacitor and thus may reduce the average voltage even in the established regime (i.e. when the capacitor is almost fully charged)[23]. In the other hand, even below the threshold voltage, a small current can flow through the diodes, and charges the storage capacitor, since the diode presents an exponential characteristic (and not a piecewise model). Thus the maximum voltage can be higher than the the source maximum voltage reduced by the threshold voltage. This signifies the leakage current is more critical for final voltage than the threshold voltage for the tested PG. The difference between the low leakage Schottky diode and the $p-n$ junction diode is small.

One can note the simulated maximum voltage for high leakage diode (`1PS76SB10`) is significantly lower than the voltage obtained with the other diodes. This is attributed to the really high leakage current of this diode (Table 1). Concerning the agreement between simulation and experiment, the shape of the curve and the values are close to each other for low leakage diodes,

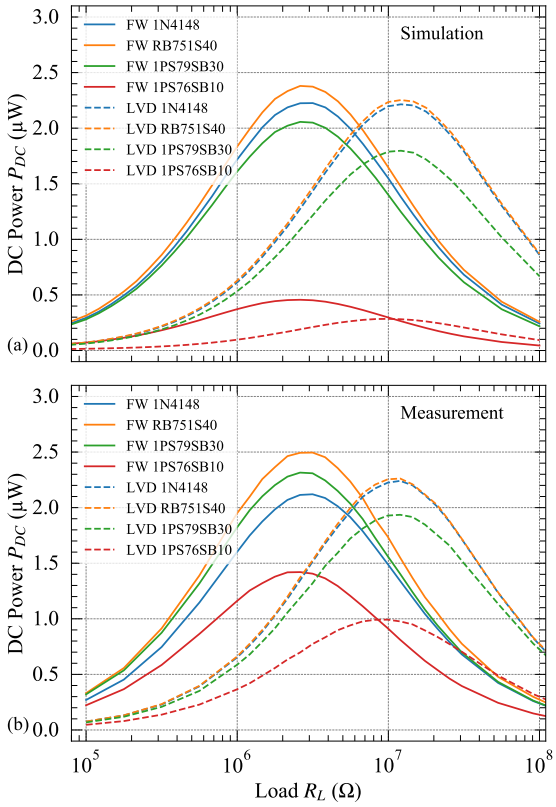

Figure 8: Power of the DC component as a function of the resistive load for different rectifier topologies and for two diode reference (a) in simulation (b) in measurement. `FW` stands for fullwave rectifier, full lines, and `LVD` stands for Latour voltage doubler, dashed lines.

indicating the simulation can predict accurately the output voltage. A discrepancy is visible for the high leakage diode (`1PS76SB10`), where in that case the simulated maximum voltage is two times lower than the measured one. This may be due to a real characteristic which is not as leaky as predicted by the datasheet.

Like a PG connected directly to the load without rectifying circuit, the average power depends on the resistive load connected to the capacitor. The goal is then to maximize the power transfered to the load, that means to maximize the dissipated power. They are two possibilities to compute the power, depending on which power we consider. The average power can be calculated using the following formula:

$$P_{ave} = \frac{1}{t_2 - t_1} \int_{t_1}^{t_2} \frac{(v(t))^2}{R_L} \, \mathrm{d}t \tag{5}$$

Nevertheless, this definition considers the power contribution of all frequency components. In the case of a rectifier, it is more relevant to consider the power of only the DC-component, calculated using the formula:

$$P_{DC} = \frac{V_{ave}^2}{R_L} \tag{6}$$

Both average and DC powers are supposed to be equal when the rectifier output voltage reached the steady state regime, showing a small ripple since the signal is almost constant.

Fig. 8 shows the DC power P_{DC} as a function of the resistive load for different rectifier topologies and diode references. The shape of the $P_{DC}(R_L)$ curve is very similar to the case without rectifying circuit as it presents a maximum for a given value of load called R_L^{DC}. The

Table 2: Summary of the computed and measured optimal load and power at optimal load for different topologies of rectifier and diodes references.

	Fullwave rectifier				Voltage doubler			
	Computation		Measurement		Computation		Measurement	
Diode reference	R_L^{DC}	P_{DC}^{max}	R_L^{DC}	P_{DC}^{max}	R_L^{DC}	P_{DC}^{max}	R_L^{DC}	P_{DC}^{max}
`1N4148`	2.84 MΩ	2.22 µW	2.94 MΩ	2.11 µW	12.3 MΩ	2.21 µW	11.1 MΩ	2.23 µW
`RB751S40`	2.81 MΩ	2.37 µW	2.83 MΩ	2.49 µW	12.2 MΩ	2.25 µW	10.9 MΩ	2.25 µW
`1PS79SB30`	2.74 MΩ	2.05 µW	2.70 MΩ	2.30 µW	11.5 MΩ	1.79 µW	11.2 MΩ	1.93 µW
`1PS76SB10`	2.53 MΩ	0.46 µW	2.49 MΩ	1.42 µW	9.8 MΩ	0.28 µW	9.0 MΩ	0.99 µW

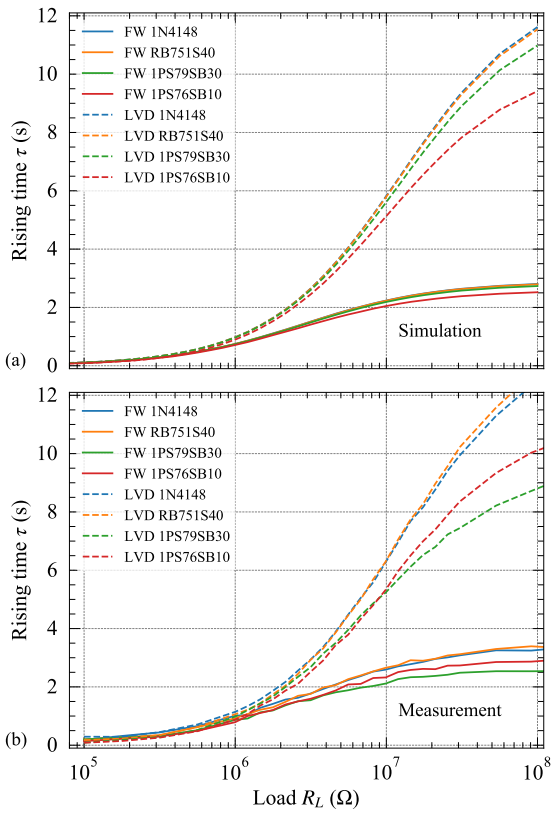

Figure 9: Rising time as a function of the resistive load for different rectifier topologies and diode references (a) simulation (b) experiment. `FW` stands for fullwave rectifier, full lines, and `LVD` stands for Latour voltage doubler, dashed-dotted lines.

optimal load and the power at this load are summarized in table 2. For both topologies of rectifier, a higher power is obtained when using the diode with the smaller leakage current. Except the high leakage current diode (`1PS76SB10`), the maximum power and optimal load are similar for all other types of diodes and are quite well predicted by the simulation. This shows, in the case of adapted diodes, that the topology of the rectifier is not critical in order to get the maximum power. The optimal load for the fullwave rectifier is higher than the optimal load without rectifier, 2.74 MΩ instead of 1.72 MΩ, but lower than for the voltage doubler (10.5 MΩ). This value of the optimal load for the fullwave bridge is consistent with the theoretical value given by Badel *et al*[15]:

$$R_{L-FW}^{DC} = \frac{\pi}{2C_{int}\omega_0} \tag{7}$$

which gives a numerical value of 2.86 MΩ. This indicates the topology of the rectifier largely modifies the optimal load. The maximum power, 2.49 µW for the fullwave rectifier using `RB751S40` diodes, has to be compared to the maximum power without rectifier (4.29 µW) which gives a efficiency of 57 % even for the "best" rectifier. For the "worst" rectifier, the voltage doubler using `1PS76SB10` diodes, the efficiency is 23 % which corresponds to a 2.5 factor on the maximum power value, which is far from being negligible.

When the capacitor is initially discharged, it takes some time to the PG to charge the capacitor to the final voltage. The Fig. 9 shows the rising time as a function of the resistive load for different topologies of the rectifier. For a given type of rectifier, the choices of the diode does not influence significantly the rising time. The rising time increases with the load value because the final voltage also increases. This comes from the fact that, to charge the capacitor using a generator with a capacitve internal impedance, at each alternance only a small fraction of the open circuit voltage is transmitted to the storage capacitor[24]. As a consequence, to reach the steady state voltage, an high number of period is necessary. The difference between the two topologies of rectifier is clear: the rising time is approximately 4 times higher for the voltage doubler. Results given by both simulation and experience are very close to each other.

3.3 Influence of the internal impedance of the PG

Depending on the PG characteristics, namely the dielectric permittivity or thickness of the active material, the surface or shape of the electrodes, the internal impedance value may change drastically. For example, in the case of ZnO-NW or AlN based generators[25,10], the internal capacitance value is relatively small compared to PZT based generators[26].

Fig. 10a shows the average voltage as a function of the resistive load, for different values of the internal capacitance of the PG, for the fullwave rectifier using `1N4148` diodes. The extraction of the average voltage has been made using the same procedure described in section 3.2. For values of the internal impedance from 10^{-8} F to 10^{-6} F, the same shape is obtained. For low resistive load value the voltage is small, then the voltage starts to increase when the resistive load is closed to the optimal load and finally the average voltage tends a limit which corresponds to the open circuit voltage. For a capacitance value of 10^{-9} F, the shape is similar but the average voltage seems to tend to a lower value than the open circuit voltage. This may be explained by the leakage current of the diodes, even very low but not negligible compared to the current provided by the PG.

Using the average voltage, the power of the DC component can be computed (Fig. 10b). When the internal impedance increases, (i) the maximum power increases and (ii) the optimal load decreases which is consistent with equations (2) and (7) respectively.

In order to see the effect of the diodes, simulations have been performed for different diodes, for the fullwave rectifier and as a function of the resistive load, over a range of internal capacitance from 10^{-9} F to 10^{-6} F. The power of the DC component has been extracted as a function

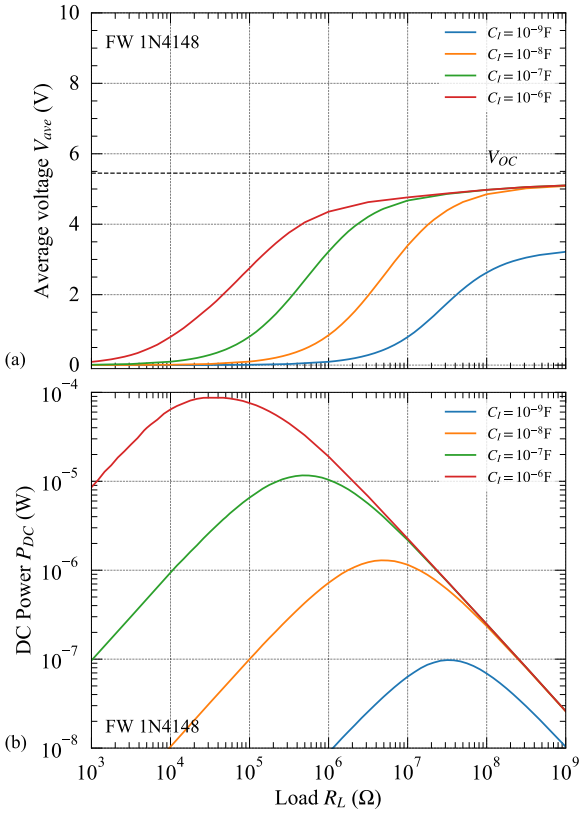

Figure 10: (a) Average voltage and (b) power of the DC component as a function of the resistive load, for different values of the internal capacitance of the PG.

of the resistive load using the procedure described previously. The maximum of this curve and the corresponding optimal load can thus be obtained for each value of the internal capacitance. Normalization of the maximum power has been done by dividing the maximum of the $P_{DC}(R_L)$ curve by the maximum AC power given by equation (2). Normalized maximum power and optimal load are presented Fig. 11.

Depending on the diode reference, corresponding to a given threshold voltage/leakage current couple, the normalized power shows a maximum for a different value of the internal capacitance (Fig. 11a). For low values of the internal capacitance, 10^{-9} F for example (signifying a PG which cannot provide a high level of current), the best choice for the diode is to have the smallest leakage current as possible even if the threshold voltage is high (for example the `1N4148` diode). For this low value of internal capacitance, `1PS79SB30` and `1PS76SB10` present a so high leakage current that the harvested power is almost null. On the other hand, for a relatively high value of the internal capacitance, 10^{-6} F for example (signifying a PG which can provide a larger amount of current), the best choice is to have the smallest threshold voltage as possible even if the leakage current is high (for example the `1PS76SB10` diode). This shows that, depending of the internal capacitance, one parameter of the diode, leakage current or threshold voltage, is the dominant limiting factor. The choice of the diode is thus critical and depends on the internal capacitance of the PG.

The optimal load, for which the maximum power is obtained, is reported Fig. 11b. The optimal load decreases when the internal capacitance increases and almost no difference is visible when the diode changes. The discrepancy at low values of the internal capacitance, for example in the range $[10^{-9}\,\text{F}, 10^{-8}\,\text{F}]$ for the `1PS76SB10` diode, mainly comes from the very low value of the power (Fig. 11a) and thus no clear maximum of power is visible, and the corresponding optimal load is not following the same tendency as with the other diodes.

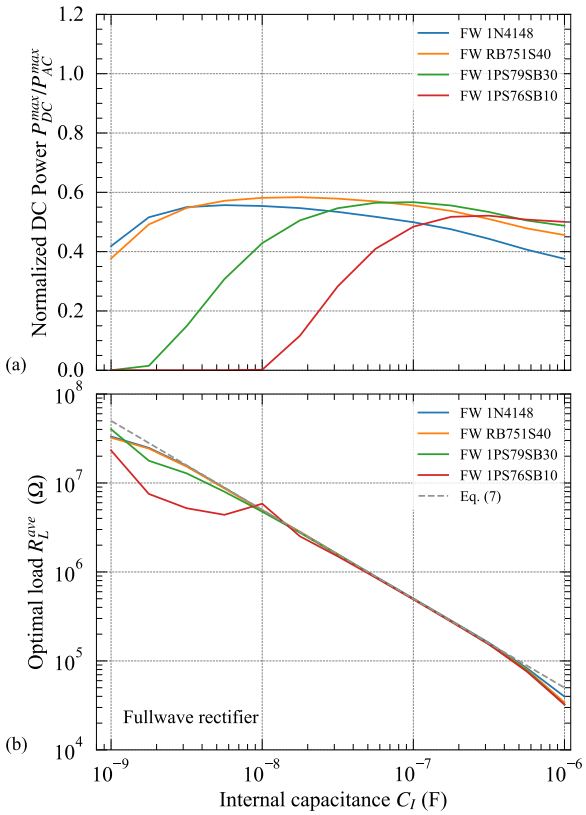

Figure 11: (a) Normalized maximum power and (b) optimal load as a function of the internal capacitance of the PG for the fullwave rectifier and the different diodes. Dashed line corresponds to the optimal load computed using (7).

Nevertheless, for this range of internal capacitance, low leakage diodes (1N4148 or RB751S40) would be preferable since the power is higher and in that case, the optimal load is correctly predicted.

4 Conclusion

In this paper, different topologies of rectifier, fullwave rectifier and voltage doubler, using different diode references, having various leakage currents and threshold voltages, have been studied. The rectifiers have been connected to a piezoelectric generator having a capacitive internal impedance. The theoretical study has been confirmed by experimental tests carried out with a PZT buzzer submitted to a controlled force. We show that the topology of the rectifier slightly influences the optimal load, at which the average power is maximal, but has only a small influence on the optimal power value. The choice of the topology is thus mainly dependent on the output voltage needed for the application.

Concerning the effect of the diode reference, the leakage current and threshold voltage are linked to each other, the lower the leakage current, higher the threshold voltage. In our case, the leakage current is the most limiting factor and must be as low as possible. On the contrary, the threshold voltage is less critical. Between the highest and lowest efficient AC/DC converter, a 2.5 factor is observed highlighting the importance of minimizing the leakage current.

We also show the internal impedance of the PG must be taken into account for the choice of the diode. Low threshold voltage diodes are more appropriate to high internal capacitance and low leakage current are preferable for low internal capacitance value.

Author contributions

K.N. and G.P.V designed the experiments. K.N. performed the simulations, measurements, data analysis and did the drafting of the manuscript. G.P.V. and D.A. did critical revisions of the manuscript and funding acquisition. All authors have read and approved the final manuscript.

Data availability

The data that support the findings of this study are available from the corresponding author upon reasonable request.

Acknowledgement

This project has received funding from the ECSEL JU under grant agreement N°692482. This JU receives support from the European Union's H2020 research and innovation program and France, Netherlands, Denmark, Belgium, Germany, Czek Republic, Spain. The Authors are also grateful for the supports from Region Centre (MEPS project 2015-2018) and National Research Agency (ANR-14-CE08-0010-01). The authors would like to thank Henrik Zessin, Vesa-Pekka Torvinen and Peter Spies, from Fraunhofer Institute for Integrated Circuits IIS, for providing the rectifiers.

Conflict of interest

The authors declare no conflict of interest

References

[1] G. Zhu, A. C. Wang, Y. Liu, Y. Zhou, Z. L. Wang, Functional electrical stimulation by nanogenerator with 58 V output voltage, Nano Letters 12 (6) (2012) 3086–3090. doi:10.1021/nl300972f.

[2] C. Opoku, A. S. Dahiya, F. Cayrel, G. Poulin-Vittrant, D. Alquier, N. Camara, Fabrication of field-effect transistors and functional nanogenerators using hydrothermally grown ZnO nanowires, RSC Adv. 5 (2015) 69925–69931. doi:10.1039/C5RA11450K.

[3] R. Tao, M. Parmar, G. Ardila, P. Oliveira, D. Marques, L. Montès, M. Mouis, Performance of ZnO based piezo-generators under controlled compression, Semiconductor Science and Technology 32 (6) (2017) 064003. doi:10.1088/1361-6641/aa691f.

[4] N. Gogneau, N. Jamond, P. Chrétien, F. Houzé, E. Lefeuvre, M. Tchernycheva, From single III-nitride nanowires to piezoelectric generators: New route for powering nomad electronics, Semiconductor Science and Technology 31 (10) (2016) 103002. doi:10.1088/0268-1242/31/10/103002.

[5] S. Xu, B. J. Hansen, Z. L. Wang, Piezoelectric-nanowire-enabled power source for driving wireless microelectronics, Nature Communications (2010) 93doi:10.1038/ncomms1098.

[6] Y. Hu, Y. Zhang, C. Xu, L. Lin, R. L. Snyder, Z. L. Wang, Self-powered system with wireless data transmission, Nano Letters 11 (6) (2011) 2572–2577. doi:10.1021/nl201505c.

[7] S. Roundy, P. K. Wright, A piezoelectric vibration based generator for wireless electronics, Smart Materials and Structures 13 (5) (2004) 1131. doi:10.1088/0964-1726/13/5/018.

[8] Z. Lin, J. Chen, X. Li, Z. Zhou, K. Meng, W. Wei, J. Yang, Z. L. Wang, Triboelectric nanogenerator enabled body sensor network for self-powered human heart-rate monitoring, ACS Nano 11 (9) (2017) 8830–8837. doi:10.1021/acsnano.7b02975.

[9] S. Xu, Y. Qin, C. Xu, Y. Wei, R. Yang, Z. L. Wang, Self-powered nanowire devices, Nature Nanotechnology 5 (2010) 366. doi:10.1038/nnano.2010.46.

[10] M. Marzencki, Y. Ammar, S. Basrour, Integrated power harvesting system including a MEMS generator and a power management circuit, Sensors and Actuators A: Physical 145-146 (Supplement C) (2008) 363 – 370. doi:https://doi.org/10.1016/j.sna.2007.10.073.

[11] P. Miribel-Català, J. Colomer-Fararons, J. L. Brinquis, J. López-Sánchez, Self-powered adaptive circuit sampling for a piezoelectric harvester, in: Design of Circuits and Integrated Systems, IEEE, 2014, pp. 1–6. doi:10.1109/DCIS.2014.7035581.

[12] D. Zhu, S. P. Beeby, M. J. Tudor, N. R. Harris, A credit card sized self powered smart sensor node, Sensors and Actuators A: Physical 169 (2) (2011) 317 – 325. doi:https://doi.org/10.1016/j.sna.2011.01.015.

[13] H. Wei, D. Cui, J. Ma, L. Chu, X. Zhao, H. Song, H. Liu, T. Liu, N. Wang, Z. Guo, Energy conversion technologies towards self-powered electrochemical energy storage systems: the state of the art and perspectives, J. Mater. Chem. A 5 (2017) 1873–1894. doi:10.1039/C6TA09726J.

[14] M. Balato, L. Costanzo, A. L. Schiavo], M. Vitelli, Optimization of both perturb & observe and open circuit voltage MPPT techniques for resonant piezoelectric vibration harvesters feeding bridge rectifiers, Sensors and Actuators A: Physical 278 (2018) 85 – 97. doi:https://doi.org/10.1016/j.sna.2018.05.017.

[15] A. Badel, D. Guyomar, E. Lefeuvre, C. Richard, Piezoelectric energy harvesting using a synchronized switch technique, Journal of Intelligent Material Systems and Structures 17 (8-9) (2006) 831–839. doi:10.1177/1045389X06057533.

[16] D. Guyomar, A. Badel, E. Lefeuvre, C. Richard, Toward energy harvesting using active materials and conversion improvement by nonlinear processing, IEEE Transactions on Ultrasonics, Ferroelectrics, and Frequency Control 52 (4) (2005) 584–595. doi:10.1109/TUFFC.2005.1428041.

[17] R. Srinivasan, U. Mangalanathan, U. Gandhi, L. R. Karlmarx, Bridgeless active rectifier for piezoelectric energy harvesting, IET Circuits, Devices & Systems 13 (7) (2019) 1078–1085. doi:10.1049/iet-cds.2018.5576.

[18] C.-Y. Hsieh, M. Moallem, F. Golnaraghi, Bridgeless converter with input resistance control for low-power energy harvesting applications, IET Power Electronics 8 (5) (2015) 822–830. doi:10.1049/iet-pel.2014.0283.

[19] A. S. Dahiya, F. Morini, S. Boubenia, C. Justeau, K. Nadaud, K. P. Rajeev, D. Alquier, G. Poulin-Vittrant, Zinc oxide nanowire-parylene nanocomposite based stretchable piezoelectric nanogenerators for self-powered wearable electronics, Journal of Physics: Conference Series 1052 (2018) 012028. doi:10.1088/1742-6596/1052/1/012028.

[20] Diode incorporated, https://www.diodes.com/design/tools/spice-models/, accessed: 2020-04-04.

[21] Xyce electronic simulator™, https://xyce.sandia.gov/, accessed: 2020-04-04.

[22] K. Nadaud, G. Poulin-Vittrant, D. Alquier, Effect of the excitation waveform on the average power and peak power delivered by a piezoelectric generator, Mechanical Systems and Signal Processing 133 (2019) 106278. doi:10.1016/j.ymssp.2019.106278.

[23] Z. Yang, L. Tang, L. Yu, K. Tao, K. Aw, Modelling and analysis of an out-of-plane electret-based vibration energy harvester with AC and DC circuits, Mechanical Systems and Signal Processing 140 (2020) 106660. doi:10.1016/j.ymssp.2020.106660.

[24] M. J. Kraśny, C. R. Bowen, C. Michel, J. T. Taylor, Transient analysis of a current-driven full wave AC/DC converter for indirect characterization of piezoelectric devices during energy harvesting, Energy Technology 8 (3) (2020) 1901317. doi:10.1002/ente.201901317.

[25] K. Nadaud, F. Morini, A. S. Dahiya, C. Justeau, S. Boubenia, K. P. Rajeev, D. Alquier, G. Poulin-Vittrant, Double buffer circuit for the characterization of piezoelectric nanogenerators based on ZnO nanowires, Applied Physics Letters 112 (2018) 063903. doi:10.1063/1.5018145.

[26] D. Isarakorn, D. Briand, P. Janphuang, A. Sambri, S. Gariglio, J.-M. Triscone, F. Guy, J. W. Reiner, C. H. Ahn, N. F. de Rooij, The realization and performance of vibration energy harvesting MEMS devices based on an epitaxial piezoelectric thin film, Smart Materials and Structures 20 (2) (2011) 025015. doi:10.1088/0964-1726/20/2/025015.